Colloid Polym Sci (2005) 283: 994–1006
DOI 10.1007/s00396-004-1253-6

Fabrice Gouanvé
H. Phuong-Nguyen
Zohra Ferhat Hamida
Geneviève Delmas

A new technique to characterize monomolecular micelles in random ethylene–propylene copolymers

Received: 14 May 2003
Accepted: 15 November 2004
Published online: 19 January 2005

F. Gouanvé · H. Phuong-Nguyen
Z. F. Hamida · G. Delmas (✉)
Chemistry Department, Université du Québec à Montréal, C.P. 8888, Succ. Centre ville, Montréal, Canada, H3C 3P8
Tel.: +1-514-9873000
Fax: +1-514-9874054

Abstract A new technique to investigate the nano-structure of ethylene–propylene (EP) random copolymers has been developed. It consists in the measurement of the turbidity which develops at a lower critical solution temperature (LCST) in pentane solutions. The information on the solution comes from different types of turbidity obtained during a step-by-step temperature increase. The transient turbidity (h_i) is associated with random coils (I) and structured coils (II) while the stable turbidity comes from aggregates (III). The proportion of (I), (II) and (III) depends on the solution history and on the solvent. The M_w distribution can be obtained from the set h_i (T_i) of (I). Turbidity (II) has an unexpected gap in the h_i (T_i) trace. The gap (10–20 K) is explained by the presence of two entities in solution. Their temperatures of phase separation permit their identification as monomolecular micelles, whose outer core is either E-rich or P-rich. This nano-structure is thought to exist in the solid and also in solution as a metastable state. The technique can differentiate between mobile chains in solutions (I, II) and attached chains in a network (III) through the sedimentation behaviour of the concentrated phase. Three samples with a similar (EP) content (0.75) made with different catalysts have been analysed by LCST and slow calorimetry.

Keywords LCST · Monomolecular micelle · Solids · Slow calorimetry · Network · EP copolymers

Introduction

Copolymers of ethylene (E) and propylene (P) (EP), $(\text{-}CH_2\text{-}CH_2)_n\text{-}(CH\text{-}CH(CH_3))_n$, have been extensively studied for their intrinsic fundamental properties or to extend the range of their applications. New catalysts permit the control of molecular weight (M_w) and M_w distribution, composition, length and the stereo-regularity of the sequences and as a consequence, the in-use properties of the materials. Composition analysis is usually determined in solution by FTIR, using standards characterized by other techniques such as solution ^1H and ^{13}C NMR spectroscopy [1–4]. Solid-state ^{13}C NMR also gives information on the structure, composition, chain mobility and aggregation in copolymers [5]. The techniques of X-ray photoelectron spectroscopy (XPS) [6] and of TOF–SIMS (time of flight secondary ion mass spectroscopy) [7, 8] give important information on the characteristics of random copolymers (composition, M_w, additive content, oxidation).

Analysis of the long-range order has been made by standard techniques on copolymers which keep some crystallinity when they have a low E or a low P content. Samples with more equal composition and no crystallinity at RT have been less investigated. It has been found by X-ray analysis or low-temperature ^{13}C NMR that the

orthorhombic modification of polyethylene (PE) is partly replaced in copolymers which have a low P content, by the pseudo hexagonal phase. It has been investigated previously on PE crystallized under pressure [3, 5, 9, 10].

Short-range order exists in non-crystalline samples or samples of low crystallinity. It has been studied by a variety of techniques at RT, or above the melting temperature T_m for semi-crystalline polymers [11]. The origin of the stability of strained micro-crystals and the techniques to analyse them (slow calorimetry [12–21], ^{13}C NMR [20] and FTIR [21]) were investigated in our laboratory. A short summary of the strain, of the conditions of its growth and its characterization by $\Delta H_{network}$ in slow calorimetry is given in Appendix 1.

In solution, long-range order disappears but short-range order often remains inside aggregates, stabilized by micro-crystals and entanglements. The techniques used for characterization try to eliminate the aggregates, either by changing the conditions of preparation or/and by filtration. Solution analysis is not expected to disclose any information on the segregation in the solid, since the equilibrium state of macromolecules in the solvent is usually a random coil. However, stable and solvent-specific structures formed from a dilute solution of amorphous polymers have been reported [11, 15, 16, 20].

The low compatibility of unlike segments favours the segregation of E and P chains. Morphologies resulting from this segregation have been extensively studied in block copolymers and blends. Segregation may also exist in random copolymers on a smaller scale at the surface and in the bulk. It could explain the range of properties of samples which are chemically very similar, or of those which have been submitted to different histories. This likely feature of random copolymers has not been the object of investigation in the solid before or after dissolution.

This paper reports the turbidity measurement at a lower critical solution temperature (LCST) in pentane of three non-crystalline EP random copolymers having an E content of 0.75, but with different histories. This technique has been previously used for testing the free volume theories of solutions [22–24], for M_w distribution [23–27] and for information on aggregates and cross-links [24, 28]. The focus of this paper is not on M_w distribution but on a specific molecular conformation of the chains in the solid and its stability in solution. Information on this stability is obtained through the measurement of $\Delta H_{network}$ by slow calorimetry.

Experimental

Materials

The rubber samples were given by the Bayer Cie (Sarnia, ON, Canada). They do not contain additives. Pentane is of the highest grade from Aldrich used without purification.

Apparatus

Calorimeter

The Setaram C80 is a differential calorimeter, which was used in previous works [12–19]. Its stability and sensitivity permit measurements of small signals in a low T-ramp ($v = 0.02–0.05$ K/min). Base-line fluctuations are smaller than the signals. Between RT and 250 °C, they are 2–4 μW [18], while the signals corresponding to phase changes are 10–40 μW as reported in papers on slow calorimetry. Samples are placed in glass tubes, flushed by N_2 for 30 min and sealed. Melting on a conducting substrate (Hg or stainless-steel powder) has been found to improve the heat transfer during the ramp [18].

^{13}C NMR

Solution NMR: Dilute solutions of the samples in $CDCl_3$(0.5% w/v) were analysed on a Varian instrument, at RT, after a dissolution time of 24 h. The conditions are similar to those used in [4] with more data points (68,000), 3,500 scans and 200 ppm as the sweep width. The mole% of ethylene was calculated from the area under the primary, secondary and tertiary carbon atoms (method 1 of [4]).

Solid state NMR: ^{13}C MAS spectra were obtained on a Chemagnetics CMX-300 spectrometer operating at 75.4 MHz, used previously [18]. Samples (125–300 mg) were cut into pieces, placed in 7.5-mm zirconia rotors and spun at 3,000 Hz. Cross polarization was not used; the spectra were acquired with single pulses of 90° with a recycle delay of 3 s. No differences were observed with longer delays. The spectra were deconvoluted using the Spinsight software on the spectrometer with all peaks successfully fit to Lorentzian line shapes. The relative amounts of ethylene and propylene were determined from the areas of the peaks between 30.5–33.8 ppm (CH_2) and 20–22 ppm (CH_3), respectively.

Size exclusion chromatography (SEC)

The analysis were made on a standard Waters apparatus in $CHCl_3$ at RT and in THF at 35 °C. The three columns were prepared by Waters (type Mixed-C, 60 cm). The values of M_w and M_w/M_n were obtained from calibration with standard PS samples. Comments on the $CHCl_3$ and THF solutions are given in Results.

Sonication: The generator of ultrasounds is a Heat Systems Ultrasonics (kHz). The sample is immersed in an ice bath for the duration of sonication (1 h). Calibration of the generator power is made by the time

needed to change the colour of a phtalo-cyanine solution.

Turbidity measurements

The equipment is similar to that used in previous publications [24]. A home-made oven is heated by three resistances placed around the central well. The temperature is read and recorded with a thermocouple. The temperature regulator and programmer is an Eurotherm type 822. The light is from Reichert Scientific Instrument (No 1177) and the photocell, aligned with the light, is from Silonex. The beam of light goes across the upper part of the solution. The change in transmitted light after a step of temperature corresponds to a measurable transient turbidity accompanied, in part of the measurements, by a stable turbidity.

In the usual cloud-point measurements, the temperature of the first turbidity, T_o, which is usually the only one measured, corresponds to the temperature of phase separation of the highest M_w in the sample. In previous work, we improved the technique by introducing a step-by-step temperature increase, which allows for the separation at T_i, above T_o of fractions of lower M_w with a transient turbidity peak (h_i). The set of h_i (T_i) is called a thermogram, which leads to the determination of the cumulative curves and M_w distribution [23–27], as detailed in Appendix 2. Examples of cumulative curves are given in Figs. 1, 2, 3, 4, 5 and 6. The highest temperature at which a turbidity peak is observed is T_{fin} and that when half the turbidity has evolved is $T_{1/2}$.

Techniques

The 1% solutions are prepared with two modes of dissolution namely sonication at 0 °C and heat at 60 °C. Irganox is added as antioxidant (1%). For turbidity measurements, the solutions are transferred at RT in glass tubes which are flushed with nitrogen and sealed. The temperature of the oven is run between 95 °C and 190 °C.

Turbidity at an LCST

The decrease of transmitted light measured in the thermogram corresponds to the increase of scattered light during phase separation. It is different from the scattered light in good solvents, measurable as a function of the scattering angle for M_w determination, for example. It is much larger and it evolves at temperatures specific to the E or P composition of the copolymers. phase separation at LCST has also the advantage, over that at a UCST, to lead to the rapid sedimentation of the concentrated phase because of the usually high temperatures of an LCST. On the thermogram, the turbidity peaks of each fraction do not overlap.

Transient and stable turbidity

In a molecularly dissolved solution, the droplets of the concentrated phase coalesce and phase separate as another phase. When the polymer is denser than the solvent, the concentrated phase falls at the bottom of the tube, and the tube is clear as before the T increment. The set of h_i (T_i) is the type-(I) turbidity used for M_w determination. Other solutions lack turbidity peaks on a temperature interval, leading to a cumulative curve with a gap. This turbidity set is of type (II) and this is the new result of the present work. The turbidity which remains constant isothermally is the stable turbidity (III) associated with phase-separating regions which do not coalesce into a concentrate phase and do not coalesce to sediment. Type-(III) turbidity is associated with the presence of aggregates stable in the solution. The stable turbidity which increases at each increase of T is reversible, diminishing to its original value when T is reduced. The stable turbidity is measured by the ratio

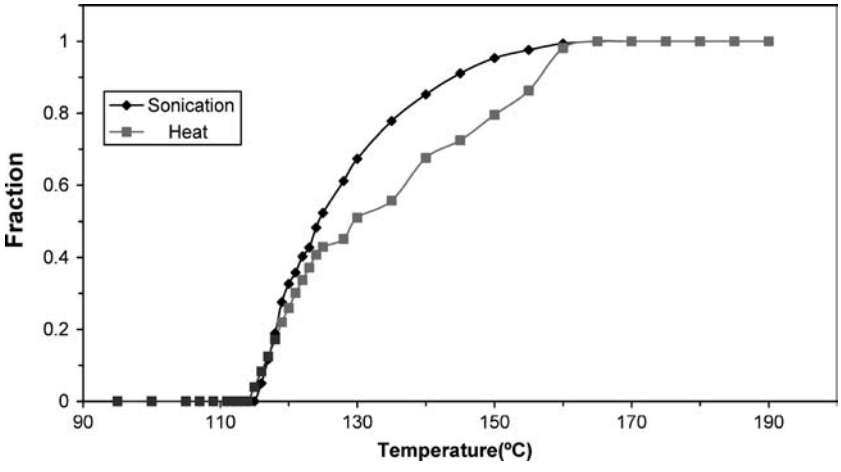

Fig. 1 Cumulative curves for sample A in *n*-pentane as a function of T. The two traces correspond to the first run after dissolution by heat (*filled square*) and sonication (*filled diamond*)

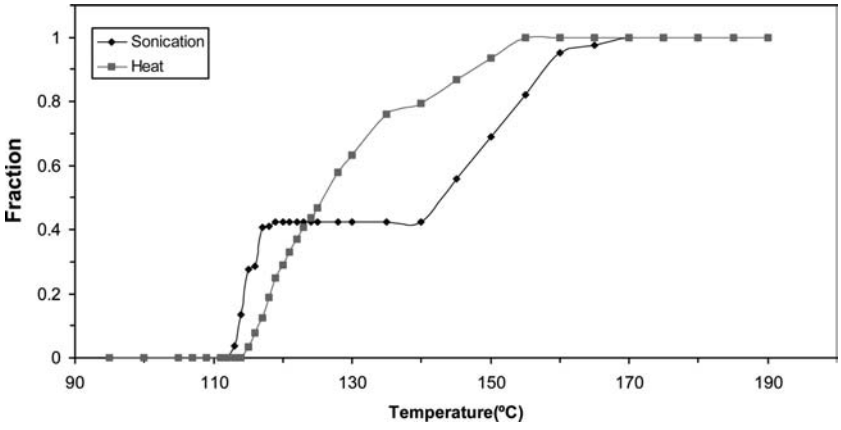

Fig. 2 Cumulative curves for sample B in *n*-pentane as a function of *T*. The two traces correspond to the first run after dissolution by heat (*filled square*) and sonication (*filled diamond*)

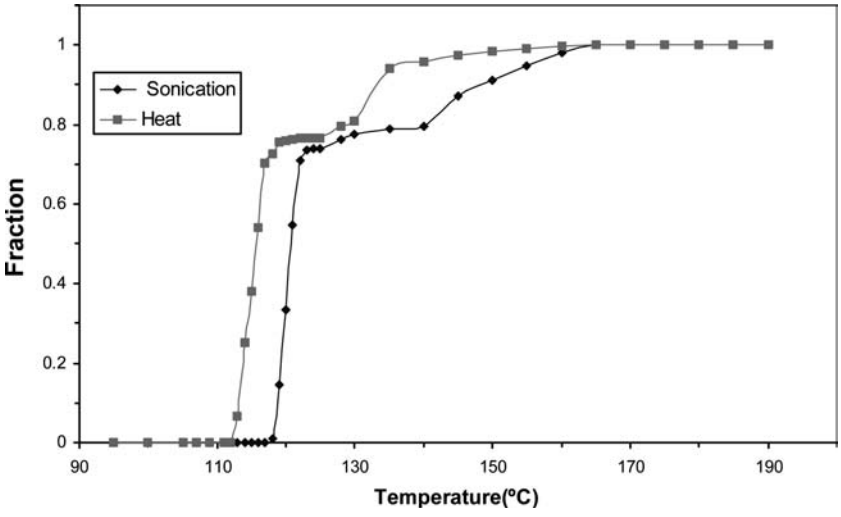

Fig. 3 Cumulative curves for sample C in *n*-pentane as a function of *T*. The two traces correspond to the first run after dissolution by heat (*filled-square*) and sonication (*filled diamond*)

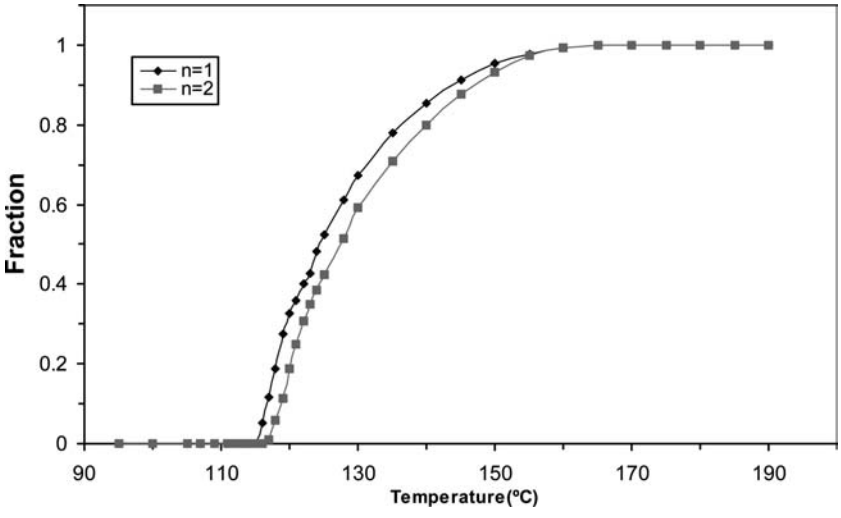

Fig. 4 Cumulative curves for sample A in *n*-pentane as a function of *T*. The two traces correspond to the first (*filled diamond*) and second (*filled square*) dissolution by sonication

$I- I_o/I_o$ where I and I_o are the intensity of the stable turbidity at T_{fin} and T_o. Cumulative curves of solutions of the three samples with different history are given in Figs. 1, 2, 3, 4, 5 and 6.

In a given solvent, the value of T_o is sensitive to M_w and in the case of a copolymer to the chemical composition [23, 26]. The constancy of T_o between the first and second run of the same sample is a good indication of

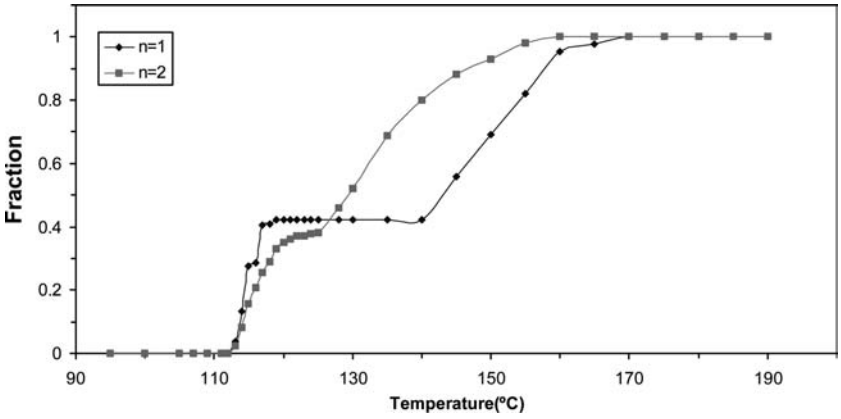

Fig. 5 Cumulative curves for sample B in *n*-pentane as a function of *T*. The two traces correspond to the first (*filled diamond*) and second (*filled square*) dissolution by sonication

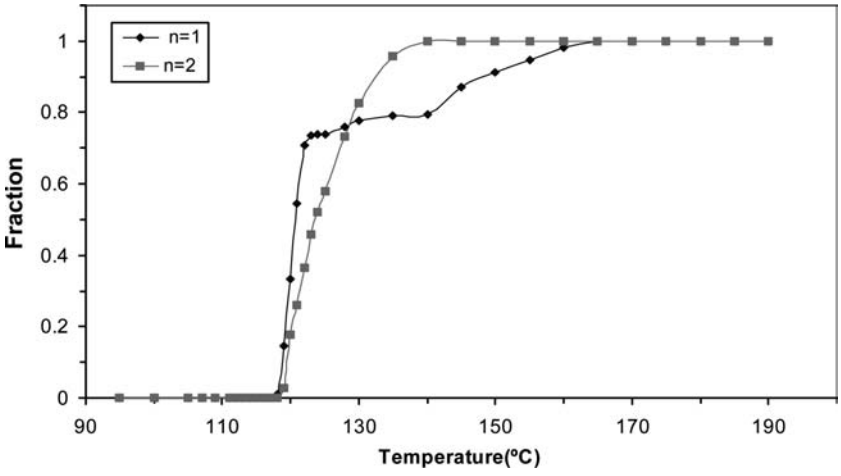

Fig. 6 Cumulative curves for sample C in *n*-pentane as a function of *T*. The two traces correspond to the first (*filled diamond*) and second (*filled square*) dissolution by sonication

the absence of degradation. In case of reticulation, the stable turbidity increases in an irreversible way.

Results

Characteristics of the samples

The characteristics of the three samples are given in Table 1. Their ethylene mole fraction (0.75) has been measured by ^{13}C NMR in the solid state and in solution by standard techniques. The norbornene incorporated in the chain is less than 0.05. The X-ray traces show no diffraction peaks. The IR spectra do not have the doublet at 720–730 cm^{-1} characteristic of the methylene in the orthorhombic cell. However, the DSC traces of samples cooled rapidly at −100 °C show two endotherms of 30–40 J/g (around −20 °C and 180 °C). Results of slow calorimetry are given in the last three columns of Table 1. Endotherms in the melt are associated with strainable short-range order, as described below and in Appendix 1.

Table 1 Characteristics of the samples by ^{13}C NMR, DSC and slow calorimetry

	^{13}C NMR Ethylene		DSC[a]				Slow calorimetry[b]		
			T (°C)	ΔH (J/g)	T (°C)	$\Delta H_{network}$ (J/g)	$\Delta H_{network}$ (J/g)	T_{final} (°C)	$T_{0.75}$ (°C)
	Solid	Solution							
A	0.74	0.72	−47	24	218	35	215	200	172
B	0.75	0.76	−25	25	240	32	240	245	201
C	0.72	0.76	−26	22	228	46	205	215	187

[a] At 10 K/min between −100 °C and 300 °C
[b] At 0.02 K/min between 30 °C and 300 °C

Table 2 Molecular weight distribution by SEC

Solvent	$CHCL_3$[a]			THF[b]		
Sample	A	B	C	A	B	C
10^{-3} M_n	84.3	165.5	217.4	289.6	226.4	293.7
10^{-3} M_w	273.8	304.9	355.8	456.7	422.1	446.7
M_w/M_n	3.24	1.84	1.63	1.57	1.86	1.52

[a] In $CHCL_3$ at room temperature
[b] In THF at 35 °C

Molecular weight distribution from SEC and the cumulative curves

Molecular weight distribution from SEC

Table 2 gives the values of M_w and M_n using $CHCl_3$ and THF as solvents. In THF, the M_w and M_n values are similar for samples A, B, C while they are different in $CHCl_3$. The differences are not unexpected. Rubber solutions in good solvents are known to contain a fraction of aggregates which can be detected by light scattering or viscosity measurements. Two opposite effects influence the M_w and M_n data: Large aggregates which stay on the filter lead to a lower value of M_w and M_n but aggregates small enough to go into solution contribute to a low elution volume fraction and higher M_w. Observations made during the preparation of the solutions are relevant to the difference between the samples. The aspect of the solution in $CHCl_3$ before filtering and the amount of polymer left on the filter were noted. The solution of sample A had some non-dissolved polymer while the others were clear. Also after filtration, the solvent flowed freely across the filter for sample C, moderately for sample B and not at all for sample A. The concentration of aggregates left on the filter would then be in the order A > B > C. The values of M_w and M_n are understandably in the reverse order (A < B < C). In THF, little difference was noted in the solutions, an observation consistent with the values of M_w and M_n similar for A, B and C. The two solvents, in spite of their similar solubility parameters, have different abilities to dissolve aggregates and the short-range order which stabilizes them. The polydispersity index (1.5–1.9) of samples B and C seem to be too low. A hypothesis on the cause is given below with the LCST analysis.

Molecular weight distribution from turbidity type (I)

A polymer or copolymer solution with a normal distribution of M_w and composition is expected to give turbidity peaks at each T increment. The high T peaks correspond to chains with lower M_w and richer in propylene segments. The cumulative curve versus T will be like the one of Fig.1 (filled diamond), which will be called a gap-free trace with type-(I) turbidity. A molecular weight distribution can be calculated only on type-(I) transient turbidity, i.e. on cumulative traces which do

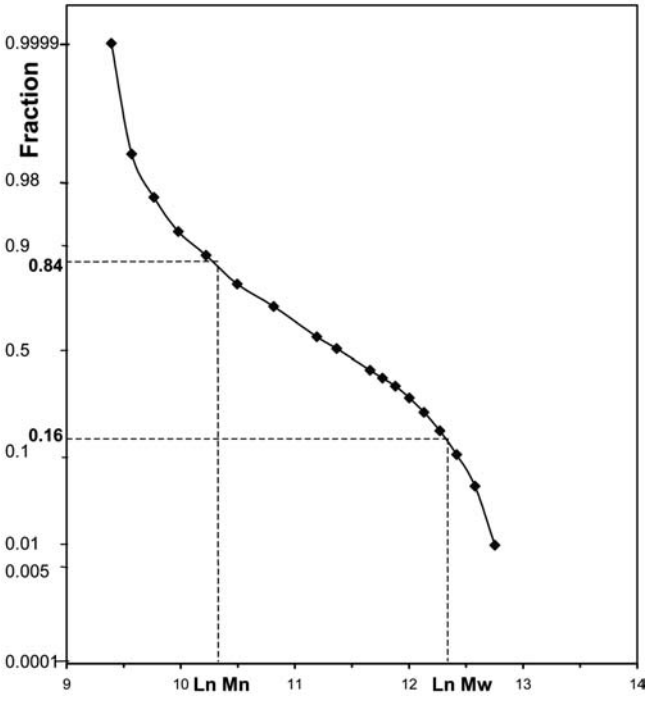

Fig. 7 Cumulative curve for sample A in *n*-pentane as a function of ln M. The trace corresponds to the second dissolution by sonication. The ordinate has a logarithmic scale. The values of ln M_w and ln M_n can be read from the figure

Table 3 Molecular weight distribution by turbidity at an LCST in pentane

Sample	A	B	C[a]	A	A
10^{-3} M_n	41	30	63	79	55
10^{-3} M_w	264	311	198	568	242
M_w/M_n	6.4	10.1	10.2	7.2	4.4
Conditions	Sonic.	Heat	Sonic.	Sonic.	Sonic.
Constants[b]	T_∞ = 106 °C B = 6,346			T_∞ = 106 °C B = 10,220	T_∞ = 99 °C B = 10,220

[a] The cumulative curve has a small gap
[b] See Eq. 3 of Appendix 2

not present a turbidity gap. Table 3 gives the values of M_w and M_n for data found in Figs. 2, 4 and 6. Three sets of the constants (T_∞ and B in Eq. 3 of Appendix 2) were used. The constants for the first three columns have been chosen because they were obtained using well-characterized narrow M_w-distribution samples of linear PE in a branched heptane [24]. Correction has been made to take into account the effect on the constants of the propylene segments [25] and the solvent volatility [23]. The fifth and sixth columns give the result with a high value of B, characteristic of volatile solvents. The values of M_w and M_n and M_w/M_n in the first and last column of Table 3 for sample A are not too different from that in $CHCl_3$, the first column of Table 2.

A cumulative curve as a function of ln M is given in Fig.7 for sample A. Details on the calculation are given in Appendix 2. Comments on the difference between the two techniques of measurement of M_w will be given below.

Table 4 Characteristic parameters of the $f(T)$ cumulative curves for sample A dissolved by heat and sonication

Dissolution by	Sample A	
	Heat $n=1$	Sonication[a] $n=1,2$
T_o (°C)	105–114	113–118
T_{fin} (°C)	160	165
$T_{1/2}$ (°C)	125	124.5–127.5
Transient turbidity type	(I)	(I)
$\sum h_i^{3/2}$ ($mm^{3/2}$)	168–226	144–407
Stable turbidity type)	(III)	(III)
$(I_o-I)/I_o$ (at T_o and at T_{fin})	0.34–0.73	0.04–0.10
Gap (°C) beginning, End	–	–
EMic, PMic, R Coils [b]	0, 0, 1	0, 0, 1

Average of several samples
[a] Some runs may have a remnant of type-(II) transient turbidity as that in Fig. 1
[b] For E-rich micelles, P-rich micelles and random coils

Cumulative curves with a turbidity gap

Effect of the sample history on the traces

Cumulative curves for the first run using the two modes of dissolution are given in Figs. 1, 2 and 3 for samples A, B and C, respectively. Figures 4, 5 and 6 compare the traces of the first and second run of the samples dissolved by sonication, also for A, B and C. These traces are for a single run but the averaged values of the parameters for the cumulative curves of two to three solutions are listed in Tables 4, 5 and 6. The rows of the tables give in turn T_o, T_{fin}, $T_{1/2}$, the type of transient turbidity ((I) or (II)) and the sum of the transient turbidity, $\sum h_i^{3/2}$. The turbidity of type (III) (or stable turbidity) is measured as the change of transmitted light $(I_o-I)/I_o$, I_o being the value (or the base line) below T_o and I that at T_{fin}. The next rows of Tables 5 and 6 give, for turbidity (II), the limits of the turbidity gap and the fraction of the polymer which has phase separated at the gap, for samples B and C, sample A having no gap [or a small one as in Fig.1 (filled square)]. The fraction of the different entities present in the solution is estimated in the last rows of Tables 4, 5 and 6, simply from the value of $\sum h_i^{3/2}$ at the temperature of the beginning of the gap. The high-T fraction is the complement to one of that listed, namely 0.61 for the third column of Table 5. Cumulative curves in Figs. 2, 3, 5 and 6 have turbidity gaps ranging from 10 K to 22 K.

General features of the traces.

1. The pentane solution of the three samples show important difference at an LCST. Sample A has no gap while samples B and C do. Furthermore, the integrated fractions of the phases separated below and above the gap are 0.4–0.6 for B and 0.8–0.2 for C (Figs. 5, 6). The sonicated solution with a small gap

Table 5 Characteristic parameters of the $f(T)$ cumulative turbidity curves for sample B dissolved by heat and ultra sounds

	Sample B			
	Heat $n=1$, 2	Sonication $n=1$	Sonication[a] $n=2$	Sonication[a] $n=2$
T_o(°C)	113–115	112–113	113–119	113
T_{fin} (°C)	160–170	170	140–150	160
$T_{1/2}$ (°C)	127	–	–	126.5
Transient turbidity type	(I)	(II)	(II)	(I)
$\sum h_i^{3/2}$ ($mm^{3/2}$)	144–148	187–412	422	418
Stable turbidity type	(III)	(III)	(III)	(III)
$I_o-I)/I_o$ (at T_o and at T_{fin})	0.52–0.73	0.02	0.02	0.17–0.43
Gap (°C) beginning	–	118–120	123	–
End	–	128–145	126	–
Fraction at gap	–	0.39–0.42	0.39	–
EMic, PMic, R Coils [b]	0, 0, 1	0.4, 0.6, 0	0.4, 0, 0.6	0, 0, 1

Average of several samples
[a] Second runs have either type-(II) or type-(I) transient turbidity
[b] For E-rich micelles, P-rich micelles and random coils

Table 6 Characteristic parameters of the $f(T)$ cumulative curves for sample C dissolved by heat and sonication

Dissolution by	Sample C		
	Heat $n=1$	Sonication $n=1$	Sonication $n=2$
T_o (°C)	111–115	119	115–119
T_{fin} (°C)	160–170	170	140–150
$T_{1/2}$ (°C)	–	–	124.5–127.5
Transient turbidity type	(II)	(II)	(I)
$\sum h_i^{3/2}$ ($mm^{3/2}$)	180–210	183–212	169–394
Stable turbidity type	(III)	(III)	(III)
$(I_o-I)/I_o$ (at T_o and at T_{fin})	0.26–0.73	0.06–0.09	0.11
Gap (°C) begining	118–121	124	–
End	128–130	144	–
Fraction at gap	0.78–0.89	0.79–0.83	–
EMic, PMic, R Coils [a]	0.8, 0.2, 0	0.8, 0.2, 0	0, 0, 1

Average of several samples
[a] For E-rich micelles, P-rich micelles and random coils

has been shown in Fig. 1 (filled diamond) to show the remnants of a gap. In other solutions of A, turbidity type (II) is not observed.

2. The mode of dissolution leads to different cumulative curves. Heat makes turbidity type (II) disappear (sample B) or reduce (sample C). The first run of sonicated solutions leads to a 20-K gap.
3. The sonicated solutions in the second run see the turbidity type (II) to be reduced (sample B) or to disappear (sample C). This is an indication that the equilibrium state of the solution leads to a type-(I) turbidity.

Other characteristics of the traces as reported in the tables are worth noting. The fraction of (I), as measured by $\sum h_i^{3/2}$ is larger, in average, for dissolution with sonication. On the other hand, tubidity of type (III) is considerably higher (5–10×) for dissolution by heat. The values of T_{fin} are higher for traces with a turbidity gap. Traces without turbidity gap are very similar in the first and second run but T_{fin} is still higher for the first run.

The values of T_o between the first and second run of the same sample, as seen on Figs. 4, 5 and 6, are indicative of no or very little degradation during the temperature ramp. There is no systematic shift of T_o for sonicated samples compared to solutions made by heat. For those, the fraction of turbidity (III), generally large, has the effect of lowering T_o. The values of T_o reported in the tables for samples A and C are somewhat lower for the solutions dissolved by heat.

Model of molecular-chain conformation

The thermogram of a homopolymer covers a range of temperature which depends on the solvent and the M_w distribution. The value of $T_{1/2}-T_o$ is a good indicator of the width of the M_w distribution. $T_{1/2}-T_o$ is 26 K and 19 K for samples whose M_w/M_n is, respectively, 8–10 and 3 [25]. For a copolymer such as an E–P copolymer, the range of $T_{1/2}-T_o$ is larger because the increase in the P concentration of the fractions adds a contribution to the shift due to lower M_w. In n-pentane, the LCST of PP is 70 K higher than that of linear PE [22] so that a small change in P concentration displaces the LCST significantly. For LLDPE, $T_{1/2}-T_o$ is 28.5 K for $M_w/M_n=2.8$ [26]. In the type-(I) turbidity, $T_{1/2}-T_o$ varies between 10 K and −20 K. On the other hand, in the type-(II) turbidity, the difference between T_o and the beginning of the gap is about 5 K. On this interval, the fraction of the turbidity which has evolved at low T is either 0.4 (sample B) or 0.8 (sample C) of the total. In the present assumption (Eq. 1 of Appendix 2), a fraction of the polymer equal to 0.4 or 0.8 has phase separated over this narrow T range. The molecules present in the solution phase separate into two packages as if those inside the package had almost the same M_w and composition.

The following model can explain some features of type-(II) turbidity. The accumulation of molecules in the two regions of turbidity outside the gap (i.e. below 120 °C and above 140 °C) is indicative of the presence of two entities in the solvent. From their temperatures of phase separation, they are E-rich molecules and P-rich molecules. The enrichment into E and P segments of the dissolved molecules is explained by the existence of monomolecular micelles whose surface is either E-rich or P-rich. These structures are stabilized by cohesive junctions made of micro-crystals or of short-range order between the chains. It is the combinatorial entropy of the random chains in the solvent which raises the LCST of lower M_w. The presence of the cohesive junctions inside the micelle limits the ability of the chains from taking their equilibrium size in the solvent. In consequence, the effect of a lower M_w on the free energy of mixing has been annulled. The monomolecular micelles can explain both the apparent absence either of lower M_w or of molecules richer in P segments in the thermogram of type-(II) turbidity.

During the polymerization, micelle or reversed micelles form spontaneously with either the E segments or P segments at the surface. These structures have a lower free energy than those of random chains since the number of thermodynamically unfavourable E-P contacts is lower. The molecules formed in the usual polymerization, have a range of E/P compositions and of segment chain lengths around the average value. The micelles may be made of molecules having a higher E content or longer E segments. The reverse micelles, in turn, would have a higher P content or longer P segments. In the presence of a solvent, on the other hand, the random coil rather than the micellar organization is the equilibrium state due to the importance of its entropic contribution to the free energy of mixing.

However, the metastable state of the monomolecular micelle can be observed and persists, in part, after a long history, as indicated by the second run of sample B (Fig. 5), where a small gap can be seen.

The difference between the two modes of dissolution is explained by the role of the temperature upon the cohesive junctions: at 0 °C, the energy developed during sonication separates the molecules of the solid but keeps the junctions non-melted. As a consequence, the molecules are found in the solvent with the organization that they have in the solid. At 60 °C on the other hand, the solution in pentane is made of several entities. Some molecules are locked in aggregates which have lost some or most of their junctions. They are seen as turbidity type (III). Other molecules diffuse through the aggregates and become random coils in the solution. Through their repetition across the network of the aggregates, the copolymer molecules lose their original organization. The higher concentration of aggregates after dissolution at 60 °C is revealed by the data of turbidity (III) in the tables reported to be, as said above, several times higher than after sonicating the solution. Interestingly, the sonicated solutions keep a low value of turbidity (III) after the long high-T treatment (about 30 h). After a residence of weeks at RT, turbidity type (III) increases in the sonicated solutions.

An indication of the presence of E-rich and P-rich sequences at the surface of the micelles is given by the values of the first and last temperatures of turbidity. The temperatures of the beginning of the gap (Figs. 6, 8, 9) are lower and T_{fin} are higher (165–170 °C) in the first run than in the second run. This is due to the replacement of E-solvent and P-solvent contacts by (EP)-solvent contacts during randomization. Note that the range of temperature of the last peaks of the thermogram in the first run is above $T_{1/2}$ of pure PP (about 154 °C). This value has been taken for solutions of iPP of M_w = 150–200,000.

Effect of the sample characteristics on the micelle stability

Effect of molecular weight

In long chain molecules which do not crystallize, entanglements, knots and stable junctions leave an organization in solution which is more stable in higher M_w samples. A simple explanation of the instability in the solvent of the structure of sample A could be due to a lower M_w. Molecular weights have been measured by SEC in polar, moderately good solvents and by LCST in a solvent whose poor quality is due to its volatility. The values of M_w and M_n of Table 2 are indeed smaller for sample A in $CHCl_3$ but in THF, they are similar to those

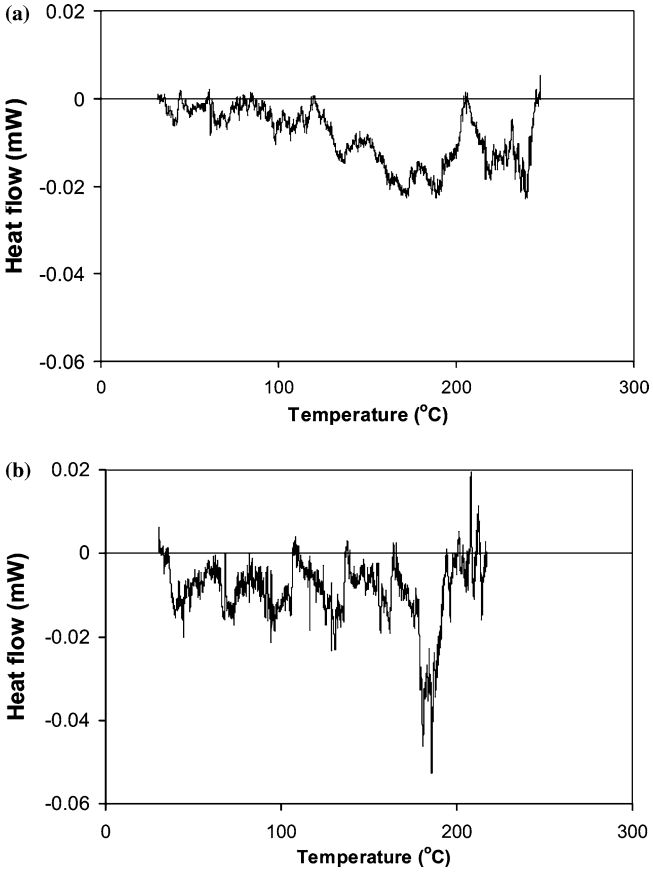

Fig. 8 Traces of slow calorimetry, between 30 °C and 270 °C, at v = 0.02 K/min. m = 20 mg, with Hg as substrate. **a** for B and **b** for A

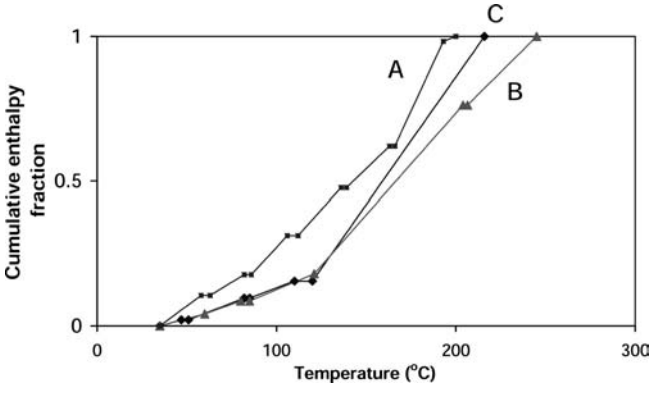

Fig. 9 Cumulative enthalpy versus temperature for traces similar to that of Fig. 8 for samples A, B and C. The slanted and flat regions correspond, respectively, to temperature range with and without signal of phase change. The values of T_{fin} and $T_{0.75}$ are in the order A < C < B

of B, C. The comparison of M_w/M_n data by SEC and LCST measurements will be given below as well as a hypothesis for the low polydispersity values obtained from SEC.

The measurement of the M_w distribution for type-(I) turbidity suffers from an ambiguity similar to that of SEC because the molecules left in the type-(III) turbidity do not enter into the analysis. The relative values for the samples are reliable, however, for the sonicated samples for which the type-(III) turbidity, as given by $I_o - I / I_o$, is small.

With these restrictions, there are interesting results concerning the values of M_n. With the first two constants, they range between 30,000 and 63,000, values considerably lower than those obtained by SEC (mostly > 200,000). The conditions of the LCST analysis (step-by-step T increase, long equilibrium time between each fraction, high T) are likely to lead, after the loss of the monomolecular micelle, to a more efficient fractionation than the columns of SEC. There may be, on the other hand, two specific reasons for the high values of M_n by SEC, namely the calibration curve and the structure of the polymer in the conditions of analysis. Calibration using the elution volume of PS in a good solvent is widely used and has been found satisfactory for comparative purposes. This calibration may give nevertheless systematically low M_n for polymers with hydrodynamic volumes smaller than that of PS. The possibility of a structure of the molecules in $CHCl_3$ and THF would not be raised without the LCST results in pentane. The anomaly in the SEC traces could escape notice because they would have a single peak, instead of the two of turbidity type (II), due to the insensitivity of the columns to the chemical nature of the moving molecules. If the solvents contain monomolecular micelles, the range of elution volumes will be small as is the range of T of turbidity type (II). The lower M_n value (84,300) for sample A, whose structure is less stable in pentane, supports the structure in the SEC solvents. Measurements of the M_w distribution by SEC in a less polar and less volatile solvent such as trichlorobenzene could confirm the above hypothesis. The sensitivity of the IR absorbance to local order is likely to also reveal the history of the sample.

Micelle stability and structure of the samples as analysed by ^{13}C NMR and slow calorimetry

^{13}C NMR

The stability of the organization in the solid is due to the E and P sequence arrangement which depends on polymerization conditions. In a copolymer $(\text{-}CH_2\text{-}CH_2\text{-})_n\text{-}(CH\text{-}CH(CH_3)\text{-})_n$, the joint segments between the $(\text{-}CH_2\text{-}CH_2\text{-})$ and $(\text{-}CH_2\text{-}CH\ (CH_3)\text{-})$ segments contain carbon atoms associated with branches and defects. They constitute the microstructure revealed on the ^{13}C NMR spectrum by small peaks situated not at the same chemical shifts as the main peaks. A meaningful comparison of the small peaks requires a very stable base line and also a homogeneous solution, as reported in the literature. Solutions in $CDCl_3$ of the A, B and C samples have been analysed in order to detect differences in their microstructure. The small peak regions of the spectra are different. They reflect in part the different solubility of the samples and the state of aggregation of the molecules. The spectra, however, do not permit to have a quantitative measurement of the sample microstructure. It is not clear if special conditions in the ^{13}C NMR equipment (measurements at low temperature) or in the solution (highly dilute solutions for instance) would lead to information on the sample microstructure.

Slow calorimetry

As a complement and alternative to the ^{13}C NMR analysis of the microstructure, the response of the samples to a very slow heating of the samples was compared. Slow calorimetry permits to characterize the network phase in the melt or in non-crystalline samples.

In previous work, the endotherm of melting, $\Delta H_{network}$, found above T_m by slow calorimetry, has been interpreted as the melting of the strained order which exists with the amorphous phase. The network phase change cannot be observed in calorimeters working in standard conditions, as explained in Appendix 1. The analysis of polyethylene samples, synthesized with different catalysts, namely Ziegler Natta (ZN) and Metallocen (MT), will be reported below because of its relevance to the question raised by the LCST results. The processing of (MT) materials presents difficulties not encountered with the (ZN) samples. The difference cannot be explained by a different long-range order. With the hypothesis that it is the entangled phase which is modified by the catalyst, the technique of slow calorimetry has been applied to the samples [29]. The network phase of MT was found to be more T-resistant than that of ZN from the range of evolution of $\Delta H_{network}$. This is an indication that the processing temperature used should be higher for MT than for ZN, an unexpected recommendation since T_m (MT) < T_m (ZN). In a semi-crystalline polymer, the strainable small range order is concentrated above T_m in the phase which has not melted. Information on the difference in processing of samples A, B and C can be obtained from their slow calorimetry traces.

Examples of these traces are given in Figs. 8a and b for samples B and A. The shape of the endotherm is as expected for the melting of short-range order in non-crystalline materials [12– 17]. The heat does not evolve between 50 °C and 220 °C with the same pattern for all the samples. In order to represent the endotherm profile, the fraction of the total enthalpy has been plotted as a function of T in Fig.9. The slanted and horizontal lines

correspond, respectively, to ranges of temperature where there is either a heat signal or none. The trace of sample A is made of five small endotherms (30–160 °C) and a final larger one (160–175 °C). The trace of sample B has two large endotherms between 140 °C and 245 °C and two smaller ones. The trace of sample C has a large endotherm (120–170 °C) and two smaller ones ending at 215 °C. A higher temperature is interpreted as more strain in the sample, corresponding to more knots among the chains. The values of $\Delta H_{\text{network}}$, T_{final} and $T_{0.75}$ of the samples are given in the last three columns of Table 1. The total enthalpies are around 240 J/g. Due to the endotherm shape, the incertitude in these values is about (± 50 J/g). Using T_{final} and the total endotherms as tracers, the stability in temperature of the monomolecular micelles are in the order A < C < B, which is the same as the stability in pentane. Traces of homopolymers usually show a single endotherm in the melt. The discontinuity in the signal observed for the present systems is likely meaningful. PP crystals melt 30 K higher than crystals of linear PE. The melting temperatures of short-range order are displaced by strain. It is likely that the low T and high T parts of the traces correspond to the melting of E-rich and P-rich junctions.Some overlapping between the high-strain junctions of one type and the low-strain regions of the other occurs. The long continuous isotherms of sample B and C may reflect larger homogeneous regions than those present in the shorter isotherms of sample A. Slow calorimetry, made over a range of v, has shown a fast decrease of $\Delta H_{\text{network}}$ when v increases [12]. Parameters of the network (T, $\Delta H_{\text{network}}$) obtained in DSC and slow calorimetry (Table 1) follow a similar pattern with an expected effect of v.

Assuming that the resistance to temperature of the strainable junctions reflects their resistance to solvent at lower temperature, we conclude that the traces in slow calorimetry give a description of the samples, which is consistent with that obtained from the LCST analysis.The present LCST study could be extended by comparing the information given by non-invasive techniques such as solid-state NMR and ATR on the nascent and solvent-treated samples. Spectra taken in our laboratory by ATR show that the history of the sample leads to significant differences in several regions of the IR spectra but specially in the 700–1,750 cm^{-1} region. The effect of changing the structure should be observed on mechanical properties or resistance to aggressive environments. The LCST technique gives valuable information on the specificity of the catalyst. Small changes in the sequence length and stereoregularity lead to a different organization in the solid state of copolymers. A correlation between other properties of the sample (mechanical properties, quality of blends, resistance to agents) with their ability to lead to a stable organization would be a suitable complement to the present work.

Conclusion

Turbidity at an LCST has been used in previous work to measure the M_{w} distribution of homopolymers and copolymers in dilute solutions where the molecules have the equilibrium random coil conformation. The equilibrium state in pentane of the present random copolymers ($E = 0.75$) is also a random coil but this state is not reached in all conditions of dissolution. Above the temperature of phase separation, three different types of turbidity can be observed, namely the transient turbidity of type (I) and (II) and the stable turbidity of type (III). Turbidity of type (I) and (II) are related with free molecules and type (III) with associated molecules in gel particles. Type-(III) turbidity is small when dissolution is achieved by sonication. The smooth cumulative curves of type-(I) turbidity lead to the determination of M_{w} distribution for the molecules outside the gel particles. The new result of this paper is the presence, in sonicated solutions, of a 10- to 20-K turbidity gap in the cumulative curves of type-(II) turbidity. From their temperatures of phase separation, the mobile entities are not copolymer molecules with the average composition but are ethylene-rich and propylene-rich monomolecular micelles present in the solvent. They are not produced at the dissolution but are tracers of the organization in the solid. This nano-organization in the nascent copolymer is due to the non-compatibility of the E and P segments. A morphology made of islands of the two kinds of micelles reduces, in the conditions of polymerization, the energetically unfavourable E-P contacts. Paradoxically, dissolution by sonication better preserves the nascent state than dissolution by heating. Measurement of M_{w} distribution by SEC suggests that in the polar volatile solvents used, the nano-structure is also conserved.

The differences observed on the three copolymers having the same overall E and P composition reflect catalyst-related subtle differences in their microstructure. The microstructure is analysed indirectly by the resistance to solvent and temperature of the entangled or network phase of the samples. The trace of slow calorimetry shows differences between the three samples, which are consistent with the difference of stability of the organization in the presence of a solvent. A higher melting-temperature range of the network phase is found for sample B, whose organization is the most stable in solution. Slow calorimetry and LCST analysis give valuable information on the entangled network phase and, consequently, on the catalyst role in the making of the phases of a polymer or copolymer.

Acknowledgements The authors acknowledge the financial support of the NSERC (General grant) and also of the support from ESTAC (Environmental Science and Technology Agency of Canada).The Bayer company (Sarnia, Ont.) gave the samples of copolymers. Dr F. Morin of McGill University, and Dr Le Than of UQAM are thanked for the ^{13}C NMR measurements and Ms J. Boivin of the University of Montreal for the SEC analyses.

Appendix 1

The concept of strain in entangled chains

Since the concept of strain will be invoked to explain the stability of the micelles in solution, some information is given here on the existence of strain in long-chain molecules. The story of nascent polymers (i.e. of polymers which have not been melted or dissolved) permits to understand the relationship between strain, entangled order and phase change: a nascent high polymer PE has a T_m of 141 °C. It presents at RT a single peak in solid state. After fusion and recrystallization, T_m is 134 °C and the ^{13}C NMR spectrum, taken in the same conditions, has two peaks. The explanation of these data is in terms of the network and strain. Before melting, the chains of the nascent material are all entangled in a physical network produced during polymerization so that there is a single distribution of chain mobility. Melting and crystallization produce two phases (crystalline and amorphous) with different mobility. When the nascent material is submitted to a fast T-ramp for melting, two correlated effects take place concomitantly, one well known, the other less: the long-range order among chains disappears at T_m and the strain grows during the expansion created by the T- ramp and by the phase change. The impossibility for the chains to reach equilibrium conformations is at the origin of the strain. Strain displaces the phase change of the remaining ordered regions at higher temperatures, as does pressure. Melting (or dissolution) is arrested and the melt (or the solution) is heterogeneous. This feature is common to all semi-crystalline polymers. Tm is lower for the recrystallized sample because the phases are more separated than in the nascent network going across the ordered regions. In non-nascent samples, the network has been reduced by crystallization but remains in the ''amorphous'' phase where short-range order remains non-melted. In non-crystalline polymers or in melts, the short-range order has been observed through different techniques [11]. Other situations, such as rapid swelling in a volatile solvent, can create, as does a fast T-ramp, non-equilibrium states and strain. The articles quoted above [12–19], give more details on the characterization of strainable order through measurement of the $\Delta H_{network}$ by slow calorimetry. The monomolecular micelles found in the present research by turbidity at an LCST, owe their cohesion and stability in the solvent to the network of the nascent copolymers, which remains imbedded in the chains. The strainable order of a copolymer is expected to give traces of melting similar to those of a homopolymer.

Appendix 2

From a thermogram to an M_w distribution

To obtain the M_w distribution from the thermogram, the following equations have been developed:

$$\Phi_i = k h_i^{3/2} \quad k = i, \quad k = final \tag{1}$$

$$\sum h_i^* = \sum h_k^{\frac{3}{2}} / \sum h_k^{\frac{3}{2}} \quad k = 1 \tag{2}$$

$$T_i = T_\infty + B M_i^{\frac{-1}{2}}$$
$$\text{or } M_i = \left(\frac{B}{T_i - T_\infty}\right)^2 \tag{3}$$

Equation 1 relates the fraction of polymer phase separating, Φ_i, and the maximum of transient turbidity h_i. Equation 2 gives the relation between h_i and the cumulative curve $\sum h_i{}^*$. The parameter k cancels in Eq.2 with the approximation that it has the same value for all the fractions. The calculation justifying the use of $h^{3/2}$ rather than h is given in [27]. Equation 3 is deduced from the thermodynamics of polymer solutions. M_i is the average M_w of the molecules which phase separate between T_i and $T_{i\text{-}n}$, with n (K) the temperature increment. The turbidity h_{fin}. is the turbidity of the last peak, i.e. of the highest temperature peak. T_∞ is the temperature of phase separation for an infinite M_w.

Values of the parameters T_∞ and B have been obtained for a variety of polymers through standards with a narrow M_w distribution [24, 25]. When those samples are not available, estimation of the constants is made on polymer fractions having a larger M_w distribution, characterized by a technique like SEC [26].

In the cumulative curves, the ordinate called fraction is equal to $\sum h_i{}^*$ and refers to the fraction of the polymer volume fraction which, at T_i, has moved in the concentrated phase.

Details of a calculation

After conversion of T_i into M_i by Eq. 3, each point of the cumulative curve is plotted on an ln graph as in Fig. 7. The points falling on a straight line indicate an ln normal distribution of the chain lengths. When the points off the straight line at low and high M_i values can be ignored, M_w and M_n are read on the linear graph at a fraction equal, respectively, to 0.16 and 0.84

[30]. The complete M_w-distribution curve can be calculated by plotting the ratio $\Delta y/\Delta x$ versus ln M where Δy and Δx are small increments along the curve, including the points off the straight line. Results for the copolymers are given in Table 3 for different values of the constants.

References

1. Randall JC (1976) J Polym Sci Polym Phys Ed 14:1693
2. Martino SD, Ketchtermans M (1995) J Appl Polym Sci 58:1781
3. Bracco S, Comotti A, Simonutti R, Camurati I, Sozzani P (2002) Macromolecules 35:1677
4. Di Martino S, Kelchtermans M (1995) J Appl Polym Sci 56:1781
5. Hu W, Srinivas S, Sirota EB (2002) Macromolecules 35:5013
6. Galuska AA, Halverson DE (1997) Surf Interface Anal 26:425
7. Galuska AA (1997) Surf Interface Anal 25:1
8. Galuska AA (2001) Surf Interface Anal 31:177
9. Wright KJ, Lesser AJ (2001) Macromolecules 34:3626
10. Basset DC, Turner B (1972) Nature 240:146
11. Keinath SEM, Miller RL, Rieke JK (eds) (1987) Order in the amorphous state of polymers. Plenum, New York
12. Phuong-Nguyen H, Delmas G (1994) J Solution Chem 23:249
13. Phuong-Nguyen H, Delmas G (1992) Macromolecules 25:411
14. Delmas G (1993) J Polym Sci Part B Polym Phys Ed 31:2011
15. Phuong-Nguyen H, Charlet G, Delmas G (1996) J Therm Anal 46:809
16. Phuong-Nguyen H, Delmas G (1995) Collect Czechoslovak Chemical Commun 60:1905
17. Bernazzan i P, Chapados C, Delmas G (2000) J Polym Sci Polym Phys Ed 38:1662
18. Zhang X, Phuong-Nguyen H, Bernazzani P, Lapes I, Delmas G (1997) Can J Chem 75: 354
19. Phuong–Nguyen H, Delmas G (1994) J Solution Chem 23:249
20. Morin FG, Delmas G, Gilson DFR (1995) Macromolecules 28:3248
21. Bernazzani P, Bich VT, Phuong-Nguyen H, Haine A, Chapados C, Dao LH, Delmas G (1998) Can J Chem 76:1674
22. Charlet G, Delmas G (1981) Polymer 22:181
23. Bohossian T, Delmas G (1992) J Polym Sci Polym Phys Ed 30:993
24. Bohossian T, Charlet G, Delmas G (1989) Polymer 30:1695
25. Barbalata A, Bohossian T, Prochaska K, Delmas G (1988) Macromolecules 21:3286
26. Barbalata A, Bohossian T, Delmas G (1992) J Appl Polym Sci 46:411
27. Bohossian T, Benoit H, Delmas G (1994) Can J Chem 72:390
28. Bernazani P, Delmas G (1997) J Therm Anal 49:449
29. Phuong-Nguyen H, Haine A, Delmas G J Materials Sci, submitted
30. Peebles LH (1971) Molecular weight distribution in polymers. Wiley, New York